Spectrochimica Acta Part A: Molecular and Biomolecular Spectroscopy 344 (2026) 126743

Contents lists available at ScienceDirect

Spectrochimica Acta Part A:
Molecular and Biomolecular Spectroscopy

journal homepage: www.journals.elsevier.com/spectrochimica-acta-part-a-molecular-and-biomolecular-spectroscopy

A lipid droplets-targeting fluorescent probe for visualized viscosity detection in cells, zebrafish and NAFLD models

Dao-Wei Li [a], Xiu-Mei Song [a], Xin-Hao Zhu [c], Heng-Xiang Zheng [a], Gao-Nan Li [a], Jiang-Wei Tian [c,*], Zhi-Gang Niu [a,*], Fa-Biao Yu [b,*]

[a] Key Laboratory of Electrochemical Energy Storage and Light Energy Conversion Matreials of Haikou City, Key Laboratory of Electrochemical Energy Storage and Energy Conversion of Hainan Province, College of Chemistry and Chemical Engineering, Hainan Normal University, Haikou 571158, China
[b] Engineering Research Center for Hainan Bio-Smart Materials and Bio-Medical Devices, Key Laboratory of Hainan Functional Materials and Molecular Imaging, College of Emergency and Trauma, Hainan Medical University, Haikou 571199, China
[c] State Key Laboratory of Natural Medicines, Jiangsu Key Laboratory of TCM Evaluation and Translational Research, School of Traditional Chinese Pharmacy, China Pharmaceutical University, Nanjing 211198, China

HIGHLIGHTS

- A newly developed viscosity-responsive fluorescent probe (**CzTP-CNPh**) has been synthesized.
- **CzTP-CNPh** exhibits high viscosity sensitivity, high selectivity, a large Stokes shift, and outstanding LDs-targeting ability.
- **CzTP-CNPh** enables the visualization of viscosity changes in LDs in cells, zebrafish and NAFLD models.

GRAPHICAL ABSTRACT

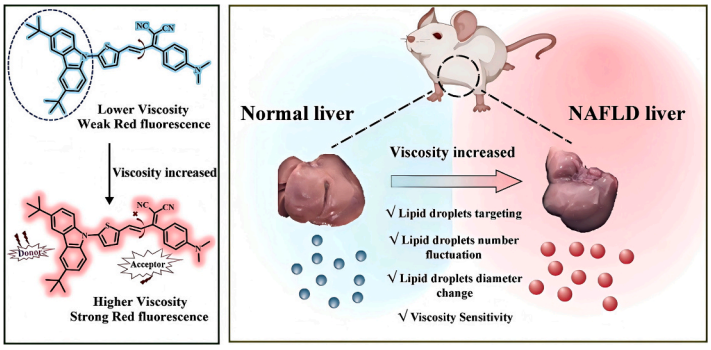

ARTICLE INFO

Keywords:
Nonalcoholic fatty liver
Lipid droplets
Viscosity
Fluorescence imaging

ABSTRACT

As a global health threat, early and effective diagnosis and treatment of nonalcoholic fatty liver disease (NAFLD) is crucial. Once the optimal treatment window is missed, NAFLD will progress to various severe and irreversible liver dysfunctions, imposing a heavy burden on patients and the medical system. Here, a novel "D-π-A" type fluorescent probe (**CzTP-CNPh**) has been successfully constructed for exploring changes in lipid droplets (LDs) viscosity during the process of nonalcoholic fatty liver development. Research results show that probe **CzTP-CNPh** exhibits excellent viscosity sensitivity, high selectivity, a large Stokes shift, outstanding LDs-targeting ability and so on. Based on these advantages, this probe enables the visualization of viscosity changes in LDs within cells and zebrafish. More importantly, imaging experiments in cellular and tissue models reveal that LDs viscosity tends to increase during NAFLD progression. This work offers the insights for enhancing the understanding of LDs in pathological processes, potentially aiding in the early diagnosis of NAFLD.

* Corresponding authors.
E-mail addresses: jwtian@cpu.edu.cn (J.-W. Tian), niuzhigang1982@126.com (Z.-G. Niu), yufabiao@muhn.edu.cn (F.-B. Yu).

https://doi.org/10.1016/j.saa.2025.126743
Received 24 June 2025; Received in revised form 22 July 2025; Accepted 25 July 2025
Available online 27 July 2025

1. Introduction

Nonalcoholic fatty liver disease (NAFLD), a serious metabolic syndrome caused by excessive lipid accumulation in liver cells, has become a global health crisis [1–3]. Over the past decades, NAFLD caused by unhealthy lifestyles has affected more than a quarter of the global population, resulting in heavy burdens on individuals and societies [4,5]. Generally, the early-stage NAFLD is reversible through lifestyle interventions like exercise and diet [6]. However, the lack of specific symptoms often delays diagnosis, leading to progression toward severe complications such as cirrhosis, fibrosis, and hepatocellular carcinoma [7–9]. Unfortunately, treatment at this stage becomes challenging and irreversible. Thus, developing novel diagnostic and therapeutic technologies is urgently required to tackle this growing threat.

Lipid droplets (LDs), spherical organelles with a hydrophilic phospholipid monolayer and hydrophobic lipid core, play a vital role in energy storage, metabolism, and signaling [10–12]. Normally, excessive lipid accumulation in LDs is a hallmark of nonalcoholic fatty liver pathology [13,14]. Viscosity, a key feature of the cellular microenvironment, maintains LDs metabolic equilibrium [15,16]. Elucidating the relationship between NAFLD, LDs, and viscosity could deepen our understanding of disease mechanisms in diagnosis and therapy [17].

Conventional viscosity detection methods (*e.g.*, rotational or capillary viscometry) face limitations such as operational complexity, low sensitivity, and incompatibility with *in vivo* visualization [18–21]. Instead, fluorescence imaging offers non-invasive, real-time monitoring with high spatiotemporal resolution [22,23]. Although numerous viscosity-sensitive LDs probes based on the twisting intramolecular charge transfer (TICT) mechanism have been developed [24–27], most suffer from poor specificity and photostability, small Stokes shifts, or aggregation-caused quenching (ACQ) effects, hindering bioimaging applications [28]. Currently, existing probes mainly focus on LDs dynamics and organelle interactions, yet their application in disease-relevant research remains underexplored [11,29]. Therefore, designing novel LDs-targeted viscosity probes is essential to unravel nonalcoholic fatty liver pathology and advance diagnostic/therapeutic strategies.

Herein, an innovative viscosity-responsive LDs fluorescent probe (**CzTP-CNPh**) has been rationally designed and constructed, with several strengths such as high viscosity sensitivity, high selectivity, good photostability, large Stokes shifts, aggregation-induced emission (AIE) effect, and low cytotoxicity. Co-localization imaging experiments demonstrate that probe **CzTP-CNPh** has the excellent LDs-targeting ability that lays a solid foundation for the specific detection of viscosity changes within LDs. Using this probe, we have also successfully achieved visualized imaging of viscosity fluctuations in cells and zebrafish. Through cellular and mouse tissue models imaging, it is revealed that the viscosity of LDs shows an increasing trend during the pathological process of nonalcoholic fatty liver. It is hoped that this work could provide some valuable insights for pathological research, drug development, diagnosis and treatment of liver-related diseases.

2. Experimental section

2.1. Reagents and instruments

All reagents were commercially purchased and used directly without further purification. The relevant instruments and equipment are detailed in the Supporting Information.

2.2. Synthesis of probe CzTP-CNPh

The synthesis route of probe **CzTP-CNPh** is presented in Scheme 1. Initially, 5-(3,6-di-tert-butyl-9H-carbazol-9-yl)thiophene-2-carbaldehyde (**CzTPF**) and 2-(1-(4-(dimethylamino)phenyl)ethylidene)malononitrile (**CN-Ph**) were prepared separately according to the methods reported in the relevant literature [30,31]. Subsequently, **CzTPF** (150 mg, 0.39 mM), **CN-Ph** (81 mg, 0.39 mM) and piperidine (6.6 mg, 77 μM) were dissolved in EtOH (15 mL). The reaction mixture was refluxed at 80 °C for 6 h. Upon completion, the reaction mixture was diluted with dichloromethane and washed with water, brine. The organic phase was separated, and the solvent was evaporated under reduced pressure. The crude product was purified by silica gel column chromatography (dichloromethane: petroleum ether = 1: 1) to give the probe **CzTP-CNPh** (red solid, 120 mg, 53 % yield). ^{1}H NMR (400 MHz, $CDCl_3$) δ 8.10–8.09 (m, 2H), 7.60–7.57 (m, 2H), 7.53 (d, J = 1.9 Hz, 2H), 7.41 (d, J = 9.0 Hz, 2H), 7.29 (s, 1H), 7.24 (s, 1H), 7.17–7.15 (m, 2H), 6.78 (d, J = 9.0 Hz, 2H), 3.10 (s, 6H), 1.47 (s, 18H). ^{13}C NMR (101 MHz, $CDCl_3$) δ 170.19, 152.67, 144.66, 144.54, 140.34, 139.07, 136.35, 131.99, 131.52, 124.28, 124.17, 123.57, 123.21, 119.84, 116.45, 114.39, 111.43, 109.91, 40.10, 31.93. HRMS Calcd for $C_{38}H_{38}N_4S$: 582.2817, found: 583.2889 ($[M + H]^+$).

3. Results and discussion

3.1. Design of the fluorescent probe CzTP-CNPh

To monitor viscosity changes within LDs, fluorescent probes must simultaneously possess excellent LDs-targeting ability and high viscosity sensitivity. In this context, carbazole was selected as an ideal fluorescent platform owing to the outstanding optical property and lipophilicity. On the other hand, the modification of the alkyl side chains would further enhance the lipophilicity of carbazole, more beneficial for the targeting of LDs. In addition, the introduction of the thiophene aldehyde group not only extends the conjugation degree of the platform, but also makes the resulting product an efficient electron donor, thereby enhancing the fluorescence performance and stability of the probe. Ultimately, through a Knoevenagel condensation reaction, the aforementioned product was connected to an electron acceptor containing a malononitrile group, constructing a "D-π-A" type fluorescent probe **CzTP-CNPh** with a strong electron push-pull effect. As a result, the molecular structure of this probe contains freely rotatable rotors that would exhibit the typical TICT effect and excellent viscosity sensitivity. In a low viscosity environment, the free rotation of the rotors will lead to energy dissipation through non-radiative transitions and thus cause fluorescence quenching.

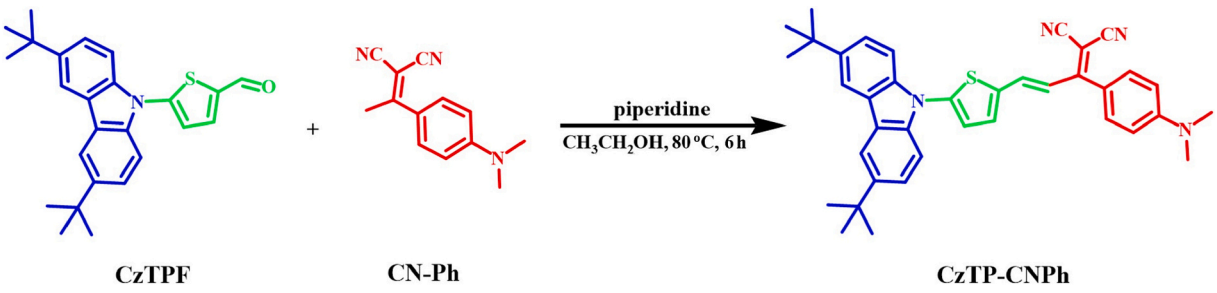

Scheme 1. Synthetic route of the fluorescent probe **CzTP-CNPh**

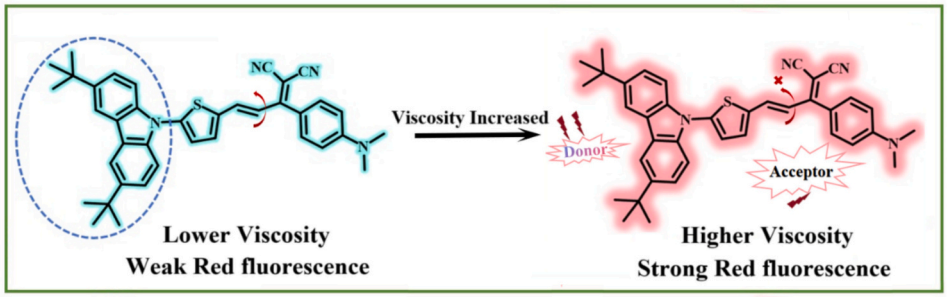

Scheme 2. Response mechanism of probe **CzTP-CNPh**

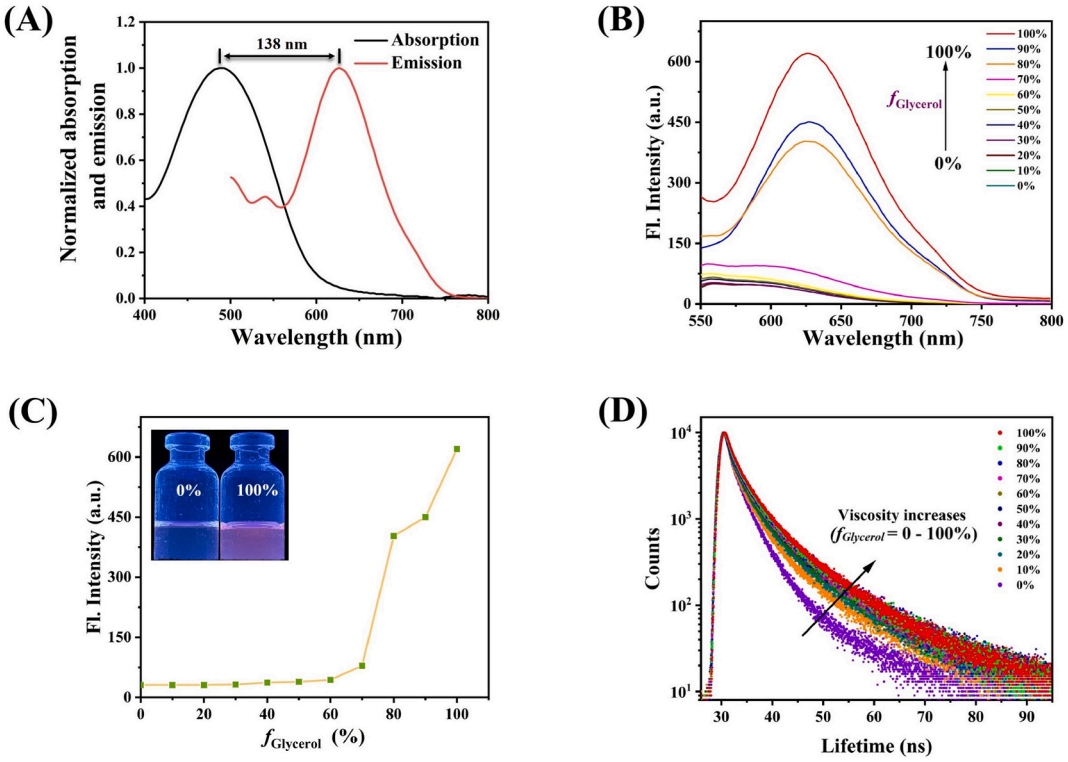

Fig. 1. (A) Normalized absorption and emission spectra of **CzTP-CNPh** (20 μM) in the glycerol solution; (B) Fluorescence spectra of **CzTP-CNPh** (20 μM) in MeOH/Glycerol solutions of different proportions; (C) The curve of fluorescence intensity at 626 nm varying with the volume fraction of glycerol; (D) The relationship between the fluorescence lifetime of probe **CzTP-CNPh** and viscosity changes.

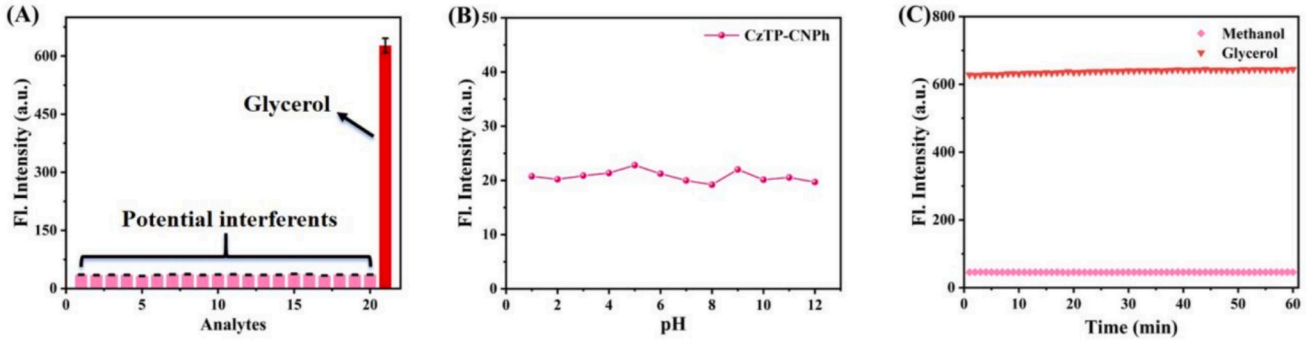

Fig. 2. (A) Selectivity of probe **CzTP-CNPh** (20 μM) at different analytes. 1. Blank, 2. K^+ (100 μM), 3. Ca^{2+} (100 μM), 4. Mg^{2+} (100 μM), 5. Na^+ (100 μM), 6. Cu^{2+} (100 μM), 7. Zn^{2+} (100 μM), 8. GSH (100 μM), 9. Hcy (100 μM), 10. Cys (100 μM), 11. $ONOO^-$ (100 μM), 12. H_2O_2 (100 μM), 13. O_2^- (100 μM), 14. ·OH (100 μM), 15. ClO^- (100 μM), 16. F^- (100 μM), 17. HS^- (100 μM), 18. SO_3^{2-} (100 μM), 19. HSO_3^- (100 μM), 20. SCN^- (100 μM), 21. Glycerol (99 %); (B) The fluorescence emission intensity of probe **CzTP-CNPh** (20 μM) in PBS at different pH (1–12); (C) Fluorescence stability of probe **CzTP-CNPh** (20 μM) in Methanol and Glycerol.

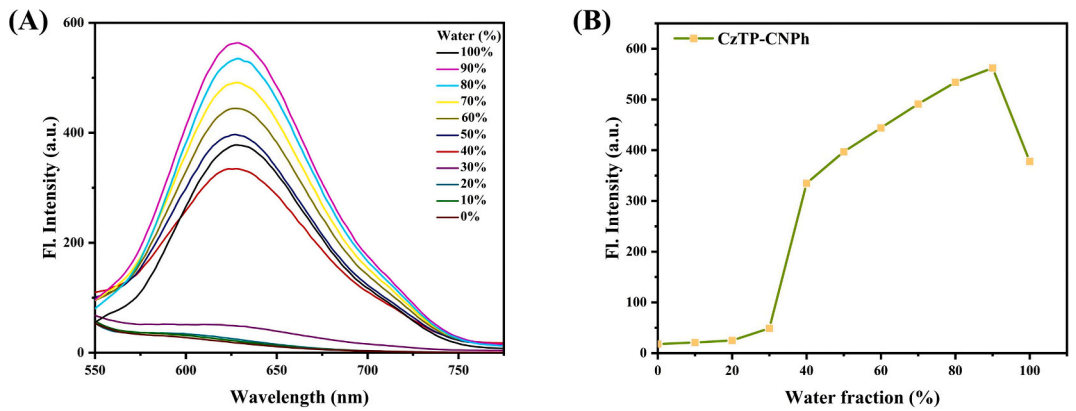

Fig. 3. (A) The fluorescence emission spectra of probe **CzTP-CNPh** (20 μM) in H_2O/DMSO solutions of different proportions; (B) The fluorescence intensity trend of probe **CzTP-CNPh** (20 μM) with the change of water volume fraction.

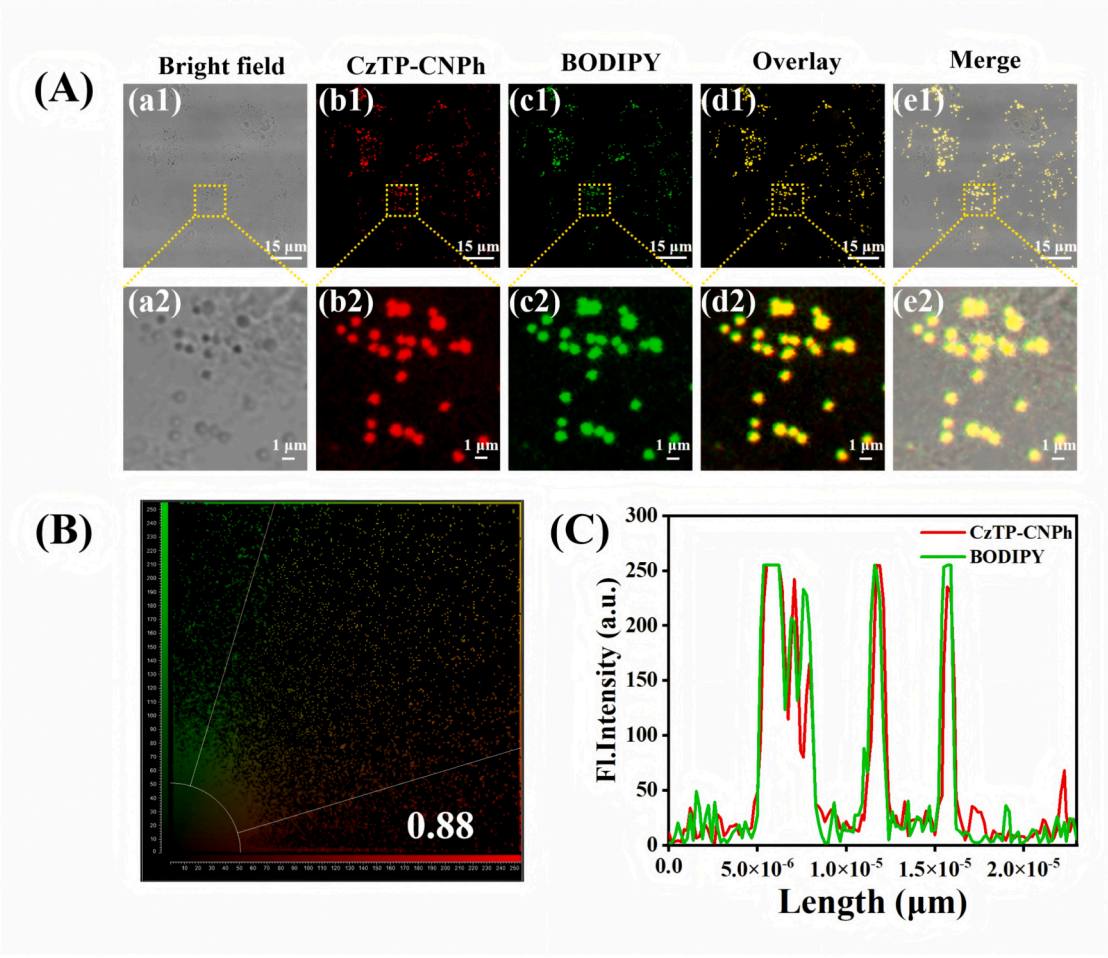

Fig. 4. Co-localization imaging experiment of probe **CzTP-CNPh**. (A) HepG2 cells were co-incubated with oleic acid (OA) for 30 min, and then **CzTP-CNPh** and commercial dye BODIPY 493/503 were added for co-localization imaging. (a1–a2): Bright field image; (b1–b2): Images of HepG2 cells stained with **CzTP-CNPh**; (c1–c2): Images of HepG2 cells stained with BODIPY; (d1–d2): Merged images of panels (b1) and (c1); (e1–e2): Merged images of panels (a1), (b1) and (c1); (B) Intensity correlation plot of **CzTP-CNPh** and BODIPY 493/503 (Pearson's coefficient, 0.88); (C) The fluorescence intensity profiles of **CzTP-CNPh** and BODIPY 493/503 within the linear ROI (region of interest) in image Fig. 4 A. **CzTP-CNPh**: λ_{ex} = 488 nm, λ_{em} = 510–600 nm. BODIPY 493/503: λ_{ex} = 493 nm, λ_{em} = 500–510 nm. Scale bar: 15 μm and 1 μm.

Conversely, high viscous conditions will impose steric restrictions on molecular rotation and consequently trigger substantial fluorescence enhancement. The corresponding response mechanism of fluorescent probe **CzTP-CNPh** is illustrated in Scheme 2. Drawing on the above considerations, we predict that this probe would exhibit excellent LDs-targeting ability and sensitive viscosity response characteristics, providing a powerful tool for in-depth study of the dynamic changes of LDs viscosity during the development of nonalcoholic fatty liver.

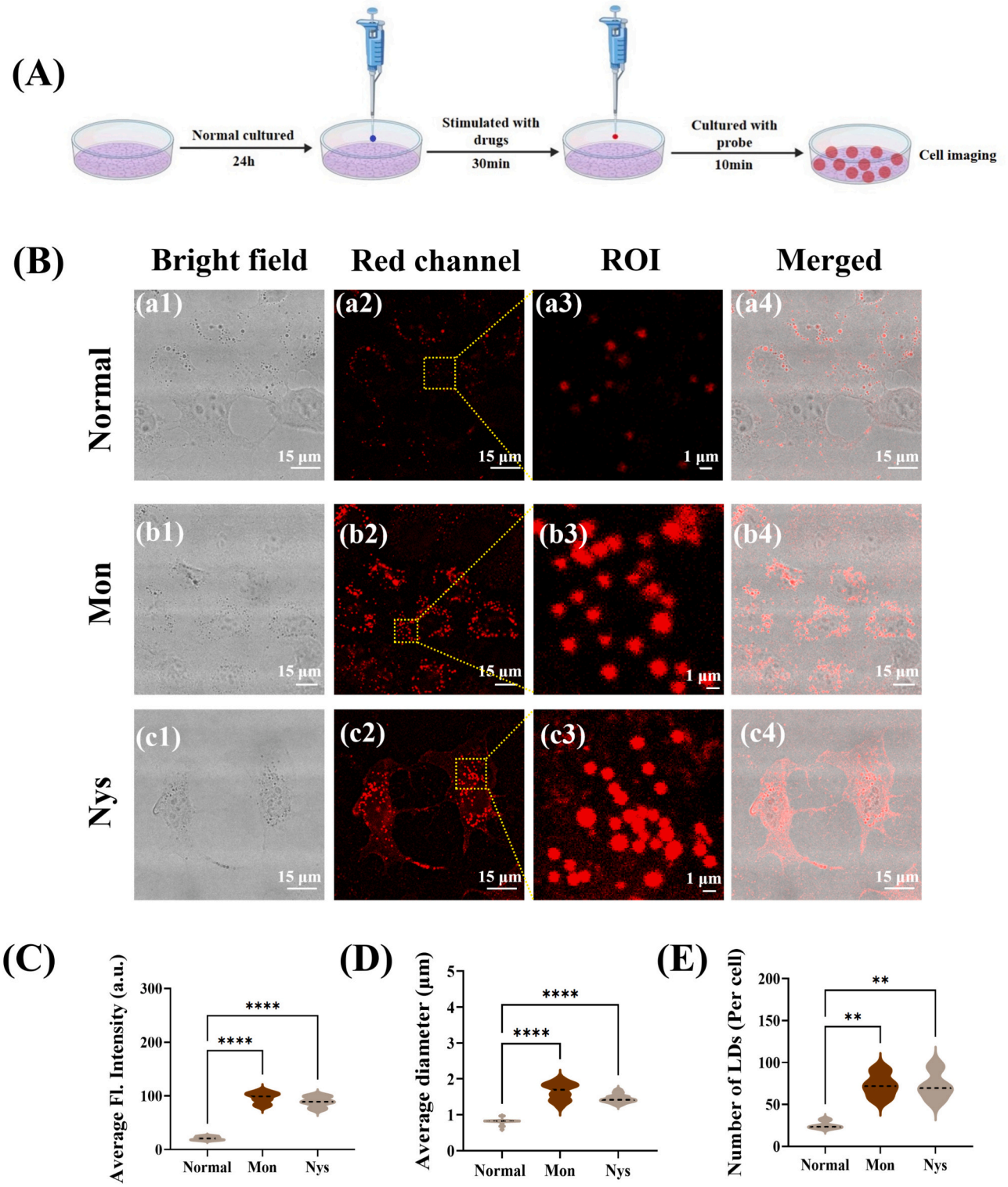

Fig. 5. (A) Flow diagram illustrating the process of cellular modeling; (B) Images of normal HepG2 cells and HepG2 cells incubated with Mon (10 μM) or Nys (10 μM) for 30 min and then incubated with **CzTP-CNPh** (10 μM) for 10 min. (a1–c1): Bright field images; (a2–c2): Fluorescence images of **CzTP-CNPh**; (a3–c3): Enlarged images of the square ROI of (a2–c2); (a4–c4): Merged images of (a1–c1) and (a2–c2); (C) Average fluorescence intensity, (D) diameter and (E) number (per cell) of LDs in HepG2 cells treated with **CzTP-CNPh** (10 μM) across various treatment groups, including the control group, Mon group and Nys group. The error bars represent thestandard deviation (±S.D.). $^{**}p < 0.01$ and $^{****}p < 0.0001$. λ_{ex} = 488 nm, λ_{em} = 510–600 nm. Scale bar: 15 μm and 1 μm.

3.2. *Spectral properties of CzTP-CNPh*

The viscosity response characteristics of **CzTP-CNPh** were first explored using a methanol-glycerol system with varying viscosities ($f_{Glycerol}$ = 0–100 %). In glycerol, the probe **CzTP-CNPh** displays a strong UV–visible absorption peak at 488 nm and a notable fluorescence emission peak at 626 nm, accompanied by a Stokes shift of 138 nm (Fig. 1A). Observably, as the viscosity of the test system continuously

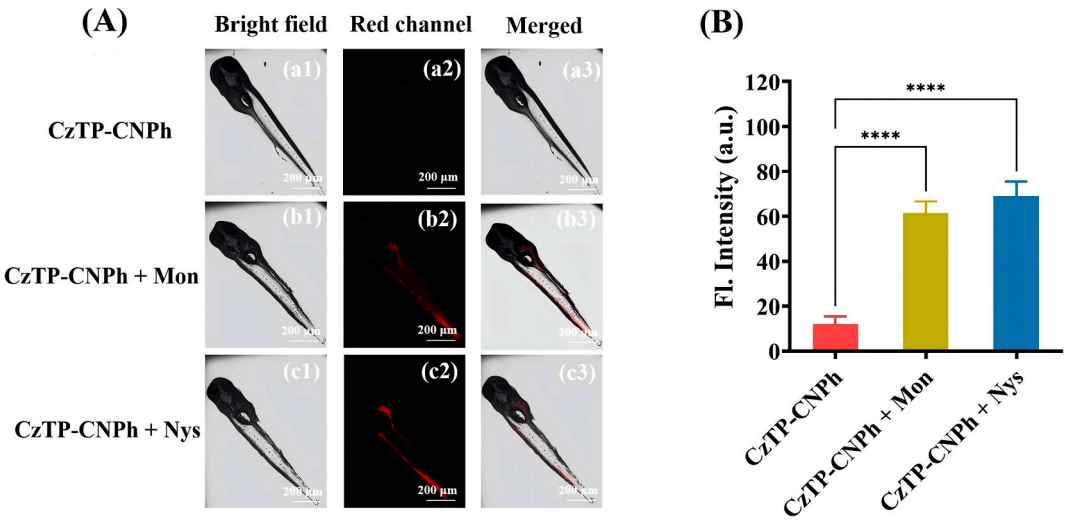

Fig. 6. (A) Confocal fluorescence image of zebrafish in different stimulation (probe only, Mon (10 μM), Nys (10 μM)). (a1–c1): The differential interference contrast image; (a2–c2): Images of red channels were collected in the range of 510–600 nm. λ_{ex} = 488 nm; (a3–c3): Merged image of (a1–c1) and (a2–c2); (B) The average fluorescence intensity from the red channel. The error bars represent the standard deviation (±S.D.). ****$p < 0.0001$. Scale bar: 200 μm. (For interpretation of the references to color in this figure legend, the reader is referred to the web version of this article.)

increases, the fluorescence intensity of the probe solution at 626 nm increases by 20-fold, reflecting a strong viscosity-dependence response (Fig. 1B and C). This significant increase in fluorescence is further supported by a distinct change in the probe solution's emission color (Fig. 1C). Under 365 nm UV-light, the probe solution exhibits negligible fluorescence emission in a low-viscosity system, but displays progressively enhanced red fluorescence as the viscosity increases. This phenomenon likely because the high-viscosity system restricts the rotation of rotors within the probe structure, thereby reducing the energy consumption during the non-radiative transition process (Fig. S1). Furthermore, there is a markedly positive correlation between the fluorescence lifetime of probe **CzTP-CNPh** and the viscosity of the test system (Fig. 1D and Table S1). These findings establish the probe as an effective tool for the specific detection of viscosity changes.

Target-specific recognition, free from interference, is essential for the probe's application *in vivo* imaging. Hence, we evaluated the probe's selectivity against various potential interferents present within the biological system (Fig. 2A). Compared with the blank group, the fluorescence of the probe remains in a quenched state after the addition of common cations, anions, reactive oxygen species, and reactive sulfur species to the test system. In stark contrast, a remarkably enhanced fluorescence emission was detected in the glycerol system, reflecting that only viscosity can selectively activate the fluorescence emission of the probe. In other words, the probe possesses a good selective response characteristic to the viscosity. Subsequently, the influence of microenvironmental parameters such as polarity and pH on the probe's viscosity response was also further evaluated. Although the UV–visible absorption and fluorescence emission spectra of the probe displayed slight fluctuations in solvents of varying polarity, the fluorescence emission intensity of the probe in glycerol was obviously enhanced (Fig. S2). In comparison, solvent polarity exerts negligible effects on the probe's fluorescence, confirming viscosity as the dominant factor driving emission enhancement. Also, the fluorescence intensity of the probe remains stable at different pH values (Fig. 2B). Thus, both polarity and pH fluctuations do not interfere with the probe detection process. Finally, the photostability of the probe under different viscosities was investigated (Fig. 2C). Under continuous light excitation for 60 min, the fluorescence intensity of probe **CzTP-CNPh** in both methanol and glycerol did not display apparent fluctuations, ensuring the photostability of the probe in biological imaging. Collectively, these experimental results indicate the probe is capable of detecting real-time viscosity fluctuations in living systems.

3.3. Aggregation-induced emission (AIE) properties of CzTP-CNPh

To study the AIE properties of **CzTP-CNPh**, a binary mixed system consisting of DMSO (a good solvent) and H_2O (a poor solvent) was utilized for spectral testing. As shown in Fig. 3, the fluorescence intensity of the probe displays a trend of first increasing and then decreasing as the water content increases. When the volume fraction of water ranges from 0 % to 90 %, there is a clear positive correlation between the fluorescence intensity of the probe and the water content. Specifically, at water fractions below 30 %, the fluorescence intensity of probe **CzTP-CNPh** shows a slow enhancement, which may be attributed to the strong TICT effect presented in probe **CzTP-CNPh** under the conditions. Once the volume fraction of H_2O exceeds 30 %, the fluorescence intensity of probe **CzTP-CNPh** rises sharply and reaches its maximum value at 90 %. This phenomenon probably arises from probe aggregation due to poor solubility at high water fractions, inducing significant fluorescence enhancement through AIE effect. When the water content in the system exceeds 90 %, however, the fluorescence intensity signal of the probe gradually diminishes, that is the aggregation of probe reaches saturation at 90 %, where fluorescence intensity reaches its maximum peak. The results confirm that probe **CzTP-CNPh** possesses strong AIE characteristics in aqueous media, and thus has the potential for cell imaging applications.

3.4. Imaging of CzTP-CNPh in living cells and zebrafish

Before performing biological imaging, the cytotoxicity of the probe was first assessed through a standard methylthiazolyldiphenyltetrazolium bromide (MTT) test. As depicted in Fig. S3, the survival rate of HepG2 cells was detected after incubation with probe solutions at different concentrations (0–32 μM) for 24 h. Even the experimental group exposed to a high concentration of 32 μM **CzTP-CNPh** solution, the survival rate of HepG2 cells still remained above 90 %, suggesting that probe **CzTP-CNPh** has extremely low cytotoxicity that meets the requirements for *in vivo* imaging applications.

To investigate whether **CzTP-CNPh** targets cellular LDs as expected, a co-localization imaging experiment was carried out using the commercial LDs dye boron-dipyrromethene (BODIPY). The distinct LDs were observed in both **CzTP-CNPh** (red channel) and BODIPY (green

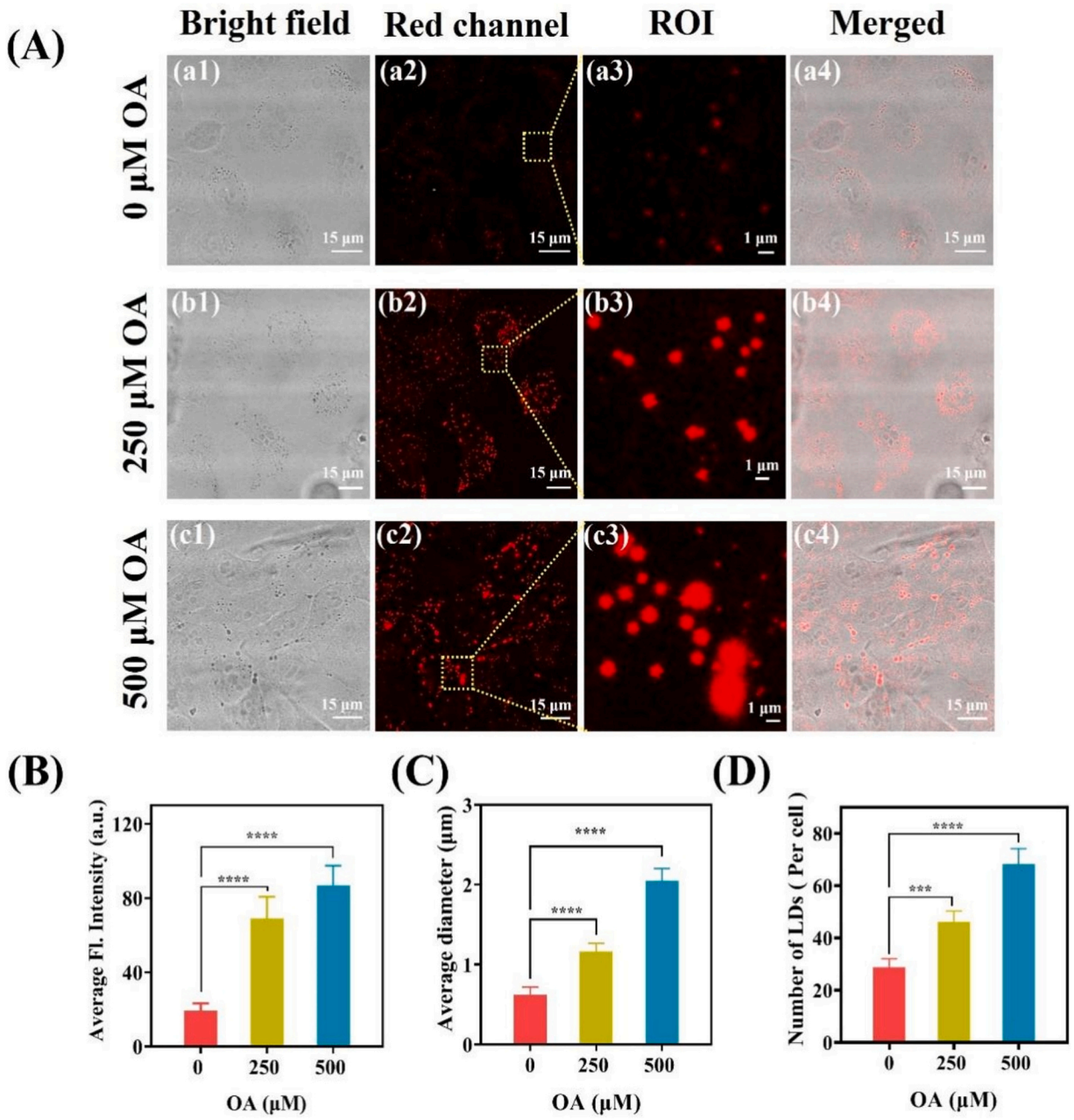

Fig. 7. (A) Images of HepG2 cells co-incubated with different concentrations of OA (0, 250 and 500 μM) for 30 min and then incubated with **CzTP-CNPh** (10 μM) for another 30 min. (a1–c1): Bright field images; (a2–c2): Fluorescence images of **CzTP-CNPh**; (a3–c3): Enlarged images of the square ROI of (a2–c2); (a4–c4): Merged images of (a1–c1) and (a2–c2); (B) Average fluorescence intensity, (C) diameter and (D) number of LDs in HepG2 cells treated with **CzTP-CNPh** (10 μM) and stimulated with varying concentrations of OA. The error bars represent the standard deviation (±S.D.). ***$p < 0.001$ and ****$p < 0.0001$. $\lambda_{ex} = 488$ nm, $\lambda_{em} =$ 510–600 nm. Scale bar: 15 μm and 1 μm.

channel), with each dye separately accumulating within the cellular LDs (Fig. 4A). The co-localization analysis revealed a clear overlap between the red and green fluorescence signals, with a Pearson's co-localization coefficient of 0.88, implying the probe's excellent targeting capability for cellular LDs (Fig. 4B and C).

In light of the satisfactory experimental results, we were eager to know whether this probe can detect changes in intracellular viscosity. Monensin (Mon) and Nystatin (Nys) are reagents that effectively increase intracellular viscosity and are commonly used in viscosity-related research. In the experiment, HepG2 cells were subjected to fluorescence imaging after being stimulated by the two reagents (Fig. 5A). Compared with the normal control group, both the experimental groups incubated with Mon and Nys exhibited remarkably enhanced fluorescence signals (Fig. 5B–C). Moreover, the changes in cellular LDs during the process can be also clearly observed through the locally enlarged images. After reagents stimulation, the diameter and number of LDs in the cells dramatically increased (Fig. 5D–E). These findings prove that Mon and Nys can effectively induce changes of cellular LDs states, while probe **CzTP-CNPh** has the capability to monitor this process. It is worth mentioning that similar phenomena were observed in the zebrafish imaging experiments, where the fluorescence intensity in zebrafish stimulated by Mon and Nys was much stronger than that in the experimental group incubated with only **CzTP-CNPh** (Fig. 6). These results suggest that probe **CzTP-CNPh** is a powerful tool for monitoring LDs-viscosity changes in cellular and zebrafish models.

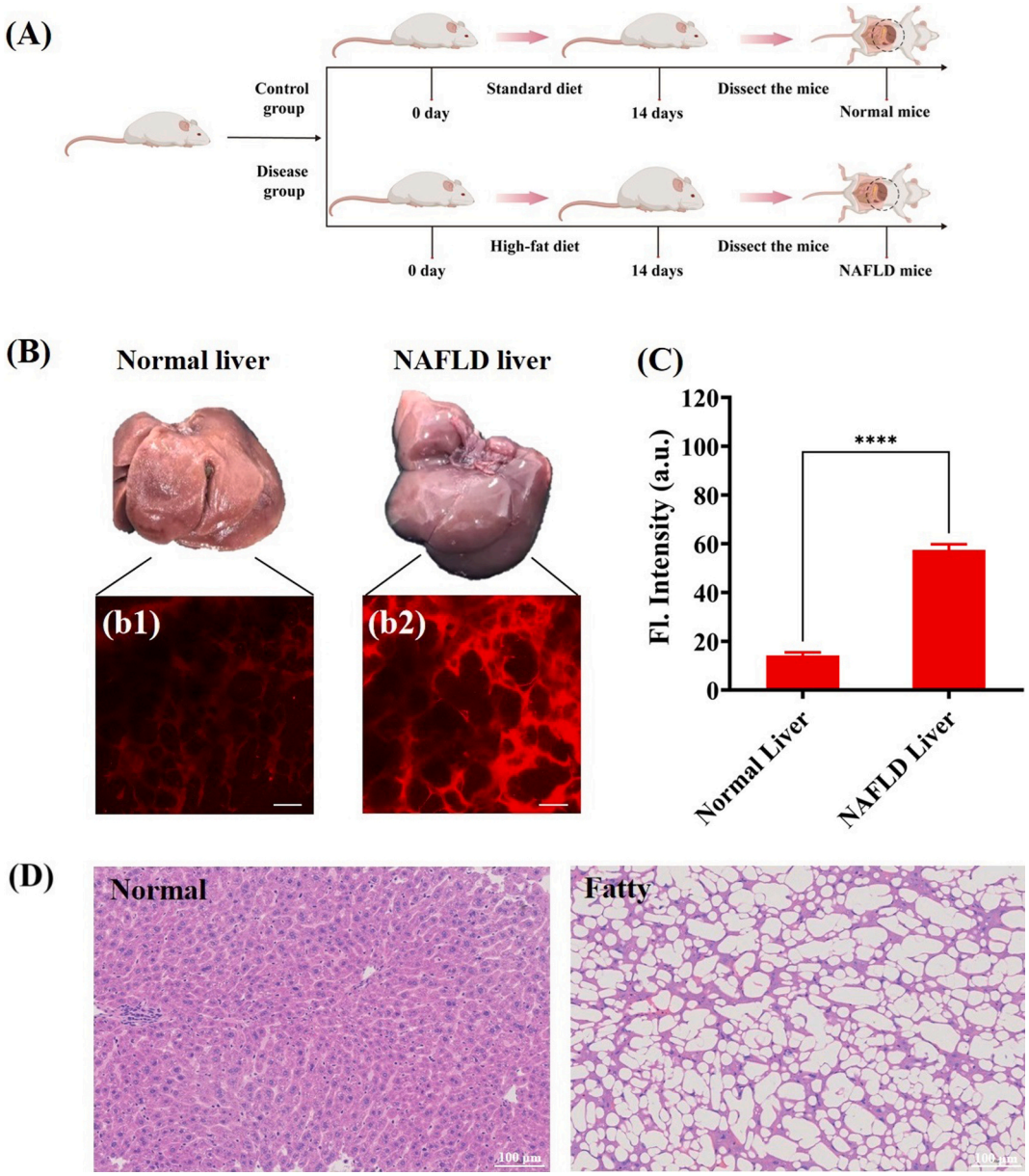

Fig. 8. (A) Flow diagram illustrating the process of mice modeling; (B) Contrast visualization imaging of tissue from normal and NAFLD mice. Fluorescence imaging of normal mouse liver (b1) and NAFLD mouse liver (b2); (C) Comparison of the difference in fluorescence intensity between normal liver and NAFLD liver under 10 μM **CzTP-CNPh** incubation condition. The error bars represent the standard deviation (±S.D.). ****$p < 0.0001$. $\lambda_{ex} = 488$ nm, $\lambda_{em} = 510–600$ nm. Scale bar: 50 μm. (D) H&E staining of liver tissues. Scale bar: 100 μm.

3.5. Visualization of LDs in NAFLD models

NAFLD, a common metabolic disorder, arises from the abnormal accumulation of LDs in hepatocytes and can ultimately lead to liver dysfunctions. Accordingly, monitoring LDs-viscosity changes in fatty liver models is crucial for understanding the pathological mechanisms of fatty liver and related liver dysfunctions. To achieve this purpose, oleic acid (OA)—a natural unsaturated fatty acid—is employed to construct a nonalcoholic fatty liver cellular model, duing to its ability to induce hepatocyte metabolic dysregulation and excessive lipid accumulation. As shown in Fig. 7A, increasing OA concentration triggered significant expansion of diameter and number of LDs, consistent with the NAFLD-associated lipid accumulation reported in the literature [15]. In other words, the nonalcoholic fatty liver cellular model was successfully constructed under the stimulation of OA. In further quantitative analysis, there is a positive correlation between the fluorescence intensity, average diameter, and number of LDs and the concentration of OA (Fig. 7B–D), signaling that the abnormal accumulation of LDs in the nonalcoholic fatty liver cellular model will lead to a notable increase in their viscosity.

Building upon the above experimental results, the NAFLD mouse model was established following the flow path in Fig. 8A and tissue section imaging was performed in Fig. 8B. As displayed in Fig. 8B, tissue imaging of mouse liver sections revealed changes of LDs are comparable to those observed in cellular models. Namely, the fluorescence intensity was markedly enhanced in NAFLD tissues relative to normal controls (Fig. 8C), confirming this consistency across experimental models. Subsequently, histological assessment was performed on liver slices from normal mice and fatty liver mice using hematoxylin-eosin (H&E) staining (Fig. 8D). The liver tissue of normal mice exhibited no obvious morphological changes, while that of fatty liver mice displayed vacuolation and slight swelling. These results demonstrate that fatty liver is

accompanied by liver injury. It can be concluded that viscosity probe **CzTP-CNPh** can effectively detects the changes of LDs in nonalcoholic fatty liver cells and tissues, which positions **CzTP-CNPh** as a powerful research tool for the diagnosis and treatment of NAFLD and related liver dysfunction.

4. Conclusions

In summary, a novel viscosity-responsive fluorescent probe, **CzTP-CNPh**, was successfully constructed based on the TICT mechanism, featuring a "D-π-A" electronic system composed of a carbazole electron donor and a malononitrile electron acceptor. Because viscosity changes restrict the rotor's free rotation within the corresponding framework, the probe exhibits high viscosity sensitivity. Additionally, the probe also features high selectivity, good photostability, a large Stokes shift, and an AIE effect, low cytotoxicity and others. Co-localization imaging experiments show that probe **CzTP-CNPh** selectively targets and accumulates within cellular LDs, establishing a basis for studying changes in the LDs microenvironment. Subsequently, the ability of the probe to detect viscosity changes in cells and zebrafish has been further validated. Importantly, the probe effectively detects an increasing viscosity trend in LDs within both the nonalcoholic fatty liver cell model and mouse liver tissue sections. This work provides a foundation for developing advanced fluorescent probes targeting the LDs microenvironment and contributes to advancing our understanding of LD-related physiological and pathological processes through enhanced diagnostic imaging and mechanistic studies, as well as facilitating the diagnosis and treatment of related diseases.

Declaration of competing interest

The authors declare that they have no known competing financial interests or personal relationships that could have appeared to influence the work reported in this paper.

Acknowledgments

This work was supported by the National Natural Science Foundation of China (22061016, 22261016, 22264013), the Hainan Provincial Natural Science Foundation of China (225RC746, 823MS042) and the Fundamental Research Funds for the Central Universities (2632024TD05).

Appendix A. Supplementary data

Supplementary data to this article can be found online at https://doi.org/10.1016/j.saa.2025.126743.

Data availability

Data will be made available on request.

References

[1] Z.M. Younossi, P. Golabi, J.M. Paik, A. Henry, C. Van Dongen, L. Henry, The global epidemiology of nonalcoholic fatty liver disease (NAFLD) and nonalcoholic steatohepatitis (NASH): a systematic review, Hepatology 77 (2023) 1335–1347, https://doi.org/10.1097/HEP.0000000000000004.
[2] W. Quan, W.H. Song, Q. Zhang, H.W. Huang, W.Y. Lin, Advances and perspectives in fluorescent probes for imaging hepatopathy-related biomarkers, Coord. Chem. Rev. 497 (2023) 215407, https://doi.org/10.1016/j.ccr.2023.21540.
[3] A. Shariq, S. Khan, S.U.R. Usmani, The role of dietary protein in mitigating the risk of nonalcoholic fatty liver disease, Nutr. Rev. 83 (2025) 1537–1539, https://doi.org/10.1093/nutrit/nuae229.
[4] E.M. Brunt, V.W.S. Wong, V. Nobili, C.P. Day, S. Sookoian, J.J. Maher, E. Bugianesi, C.B. Sirlin, B. Neuschwander-Tetri, M.E. Rinella, Nonalcoholic fatty liver disease, Nat. Rev. Dis. Primers 1 (2015) 15080, https://doi.org/10.1038/nrdp.2015.80.
[5] Z. Younossi, F. Tacke, M. Arrese, B.C. Sharma, I. Mostafa, E. Bugianesi, V.W. S. Wong, Y. Yilmaz, J. George, J. Fan, M.B. Vos, Global perspectives on nonalcoholic fatty liver disease and nonalcoholic steatohepatitis, Hepatology 69 (2019) 2672–2682, https://doi.org/10.1002/hep.30251.
[6] Z.G. Yang, Y.X. He, J.H. Lee, N. Park, M. Suh, W.S. Chae, J.F. Cao, X.J. Peng, H. Jung, C. Kang, J.S. Kim, A self-calibrating bipartite viscosity sensor for mitochondria, J. Am. Chem. Soc. 135 (2013) 9181–9185, https://doi.org/10.1021/ja403851p.
[7] S.L. Friedman, B.A. Neuschwander-Tetri, M. Rinella, A.J. Sanyal, Mechanisms of NAFLD development and therapeutic strategies, Nat. Med. 24 (2018) 908–922, https://doi.org/10.1038/s41591-018-0104-9.
[8] S.P. Zhang, P. Zhu, J.A. Yuan, K.M. Cheng, Q.X. Xu, W. Chen, Z. Pan, Y.Q. Zheng, Non-alcoholic fatty liver disease combined with rheumatoid arthritis exacerbates liver fibrosis by stimulating co-localization of PTRF and TLR4 in rats, Front. Pharmacol. 14 (2023) 1149665, https://doi.org/10.3389/fphar.2023.1149665.
[9] A.M. Diehl, C. Day, Cause, pathogenesis, and treatment of nonalcoholic steatohepatitis, New. Engl. J. Med. 377 (2017) 2063–2072, https://doi.org/10.1056/NEJMra1503519.
[10] X. Tian, D. Wu, W.H. Wei, G.F. Dai, Z.X. Li, B.H. Wang, M.M. Yu, A lipid droplets-targetable fluorescent probe for polarity detection in cells of iron death, inflammation and fatty liver tissue, Chin. Chem. Lett. 35 (2024) 108912, https://doi.org/10.1016/j.cclet.2023.108912.
[11] X.J. Zheng, W.C. Zhu, F. Ni, H. Ai, S.L. Gong, X. Zhou, J.L. Sessler, C.L. Yang, Simultaneous dual-colour tracking lipid droplets and lysosomes dynamics using a fluorescent probe, Chem. Sci. 10 (2019) 2342–2348, https://doi.org/10.1039/c8sc04462g.
[12] J.R. Zheng, S.H. Qin, L.J. Gui, H. Li, L.X. Fan, Y.F. Yang, H.Y. Chen, H. Xu, Z. W. Yuan, Light-up lipid droplets for the visualization of lipophagy and atherosclerosis by coumarin-derived bioprobe, Chin. Chem. Lett. 32 (2021) 2385–2389, https://doi.org/10.1016/j.cclet.2021.02.059.
[13] S. Zhang, B. Ji, J. Li, W.J. Ji, C.Q. Yang, L. Yang, FBXL5 promotes lipid accumulation in alcoholic fatty liver disease by promoting the ubiquitination and degradation of TFEB, Cell. Signal. 112 (2023) 110905, https://doi.org/10.1016/j.cellsig.2023.110905.
[14] F. Seebacher, A. Zeigerer, N. Kory, N. Krahmer, Hepatic lipid droplet homeostasis and fatty liver disease, Semin, Cell. Dev. Biol. 108 (2020) 72–81, https://doi.org/10.1016/j.semcdb.2020.04.011.
[15] J. Liu, M. Luo, W.J. Gao, K.Y. Duan, H.J. Bian, Z.Y. Ji, Y.H. Pan, S.Y. Wang, Y. Q. Gu, J.R. Zheng, R.X. Li, Z.W. Yuan, Dual-responsive two-photon probe for specific lipid droplets near-infrared fluorescence imaging in the brain of epileptic mice, Biosens. Bioelectron. 267 (2025) 116774, https://doi.org/10.1016/j.bios.2024.116774.
[16] M.K. Kuimova, S.W. Botchway, A.W. Parker, M. Balaz, H.A. Collins, H.L. Anderson, K. Suhling, P.R. Ogilby, Imaging intracellular viscosity of a single cell during photoinduced cell death, Nat. Chem. 1 (2009) 69–73, https://doi.org/10.1038/Nchem.120.
[17] Y.H. Wang, H.K. Guo, W. Wan, B.J. Jing, Y.L. Bai, J.L. Sun, X. Zhang, Z.M. Gao, Y. Liu, X.P. Dong, A solvatochromic and photosensitized lipid droplet probe detects local polarity heterogeneity and labels interacting proteins in human liver disease tissue, Adv. Healthc. Mater. 14 (2025) 2404713, https://doi.org/10.1002/adhm.202404713.
[18] T. Seckin, S.M. Kormaly, An easy-to-build rotational viscometer with digital readout, J. Chem. Educ. 73 (1996) 193–194, https://doi.org/10.1021/ed073p193.
[19] Á. de la Rosa, E. Poveda, G. Ruiz, R. Moreno, H. Cifuentes, L. Garijo, Determination of the plastic viscosity of superplasticized cement pastes through capillary viscometers, Constr. Build. Mater. 260 (2020) 119715, https://doi.org/10.1016/j.conbuildmat.2020.119715.
[20] J.J. Chao, H. Zhang, Z.Q. Wang, Q.R. Liu, G.J. Mao, D.H. Chen, C.Y. Li, A near-infrared fluorescent probe for monitoring abnormal mitochondrial viscosity in cancer and fatty-liver mice model, Anal. Chim. Acta 1242 (2023) 340813, https://doi.org/10.1016/j.aca.2023.340813.
[21] Y. Wei, X.Y. Zi, J. Zhai, M. Zhang, J.Q. Li, Z.L. Sun, M.Z. Ju, X. Zhang, B.X. Shen, Exploring endoplasmic reticulum dysfunction on protein phase separation using viscosity-sensitive fluorescent lifetime probe, Anal. Chem. 97 (2025) 10038–10045, https://doi.org/10.1021/acs.analchem.5c01131.
[22] J.X. Hong, X.G. Guan, Y. Chen, X.D. Tan, S.Y. Zhang, G.Q. Feng, Mitochondrial membrane potential independent near-infrared mitochondrial viscosity probes for real-time tracking mitophagy, Anal. Chem. 95 (2023) 5687–5694, https://doi.org/10.1021/acs.analchem.2c05568.
[23] D.D. Tang, N.G. Xu, Y.Y. Fu, W. Peng, J.S. Wu, H. Liu, F.B. Yu, Rationally designed an innovative proximity labeling near-infrared fluorogenic probe for imaging of peroxynitrite in acute lung injury, Chin. Chem. Lett. 36 (2025) 110082, https://doi.org/10.1016/j.cclet.2024.110082.
[24] Y. Liang, Y.P. Zhao, C.F. Lai, X. Zou, W.Y. Lin, A coumarin-based TICT fluorescent probe for real-time fluorescence lifetime imaging of mitochondrial viscosity and systemic inflammation, J. Mater. Chem. B 9 (2021) 8067–8073, https://doi.org/10.1039/d1tb01150b.
[25] Y.Y. Li, J.L. Hu, J.R. Wu, Y.R. Wang, A.H. Zhang, Y.W. Tan, Y.J. Shang, T. Liang, M. Li, Y.L. Meng, Y.F. Kang, Multifunctional fluorescence probe for simultaneous detection of viscosity, polarity, and $ONOO^-$ and its bioimaging in vitro and vivo, Biosens. Bioelectron. 254 (2024) 116233, https://doi.org/10.1016/j.bios.2024.116233.
[26] S. Ludwanowski, A. Samanta, S. Loescher, C. Barner-Kowollik, A. Walther, A modular fluorescent probe for viscosity and polarity sensing in DNA hybrid mesostructures, Adv. Sci. 8 (2021) 2003740, https://doi.org/10.1002/advs.202003740.

[27] C. Wang, W.J. Chi, Q.L. Qiao, D.V. Tan, Z.C. Xu, X.G. Liu, Twisted intramolecular charge transfer (TICT) and twists beyond TICT: from mechanisms to rational designs of bright and sensitive fluorophores, Chem. Soc. Rev. 50 (2021) 12656–12678, https://doi.org/10.1039/d1cs00239b.

[28] J.B. Ma, R. Sun, K.F. Xia, Q.X. Xia, Y. Liu, X. Zhang, Design and application of fluorescent probes to detect cellular physical microenvironments, Chem. Rev. 124 (2024) 1738–1861, https://doi.org/10.1021/acs.chemrev.3c00573.

[29] F.F. Meng, J. Niu, H.M. Zhang, R. Yang, Q. Lu, Y. Yu, Z.Q. Liu, G.L. Niu, X.Q. Yu, Simultaneous visualization of lipid droplets and lysosomes using a single fluorescent probe, Sens. Actuators B Chem. 329 (2021) 129148, https://doi.org/10.1016/j.snb.2020.129148.

[30] B. Vigante, K. Leitonas, D. Volyniuk, V. Andruleviciene, J. Simokaitiene, A. Ivanova, A. Bucinskas, J.V. Grazulevicius, Synthesis of linear and V-shaped carbazolyl-substituted pyridine-3,5-dicarbonitriles exhibiting efficient bipolar charge transport and E-type fluorescence, Chem. Eur. J. 25 (2019) 3325–3336, https://doi.org/10.1002/chem.201805323.

[31] Y.H. Yang, W.L. Cui, M.H. Wang, J.Y. Wang, Synthesis of fluorescent dyes based on the electron-withdrawing core of malononitrile and construction of viscosity-sensitive AIE probe with large stokes shift for lipid droplets imaging, Dyes Pigments 233 (2025) 112528, https://doi.org/10.1016/j.dyepig.2024.112528.